ACS APPLIED MATERIALS & INTERFACES

Research Article

www.acsami.org

Synthesis of Pt-Loaded Self-Interspersed Anatase TiO_2 with a Large Fraction of (001) Facets for Efficient Photocatalytic Nitrobenzene Degradation

Wei-Kang Wang,[†] Jie-Jie Chen,[†] Wen-Wei Li, Dan-Ni Pei, Xing Zhang, and Han-Qing Yu*

Department of Chemistry, University of Science & Technology of China, Hefei, 230026, China

ABSTRACT: TiO_2 is capable of directly utilizing solar energy for sustainable energy harvest and water purification. Facet-dependent performance of TiO_2 has attracted enormous interests due to its tunable photocatalytic activity toward photoredox transformations, but information about the noble-metal-loaded TiO_2 for its facet-dependent photocatalytic performance, especially in pollutant degradation systems, is limited. In this work, inspired by our previous theoretical calculations about the roles of the crystal surface in Pt-loaded TiO_2 in its enhanced photocatalytic capacity, TiO_2 nanocrystals with interspersed polyhedron nanostructures and coexposed (001) and (101) surfaces as a support of Pt nanoparticles are prepared in a simple and relatively green route. Also, their performance for photocatalytic degradation of nitrobenzene (NB), a model organic pollutant, is explored. The experimental results demonstrate that the NB photodegradation and photoconversion efficiencies are significantly enhanced by uniformly loading Pt nanoparticles on the crystal surfaces, but the Pt nanoparticles deposited on only the (101) surface have no contribution to the improved NB photodegradation. Furthermore, the liquid chromatography mass spectrometry results also show that NB photodegradation tends to proceed on the (001) surface of Pt/TiO_2 for the generation of nitrophenol intermediates through the photooxidation pathway. This work provides a new route to design and construct advanced photocatalysts toward pollutant photoredox conversions and deepens our fundamental understanding about crystal surface engineering.

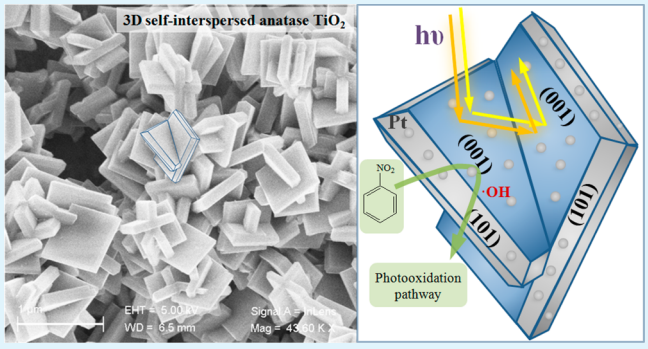

KEYWORDS: *titanium dioxide, noble-metal deposition, photocatalysis, nitrobenzene, crystal surface*

INTRODUCTION

Metal oxide semiconductor materials have wide potential applications in achieving energy storage and environmental remediation toward, for example, photocatalytic hydrogen evolution, and degradation of organic pollutants in water and wastewater.[1,2] TiO_2 is one of the most widely used photocatalysts with superior physicochemical and optical properties.[3,4] TiO_2-mediated photocatalysis has drawn considerable interests because it offers a possibility of directly utilizing solar energy and causes no new pollution in energy harvest and water purification.[5,6] Analyzing the fundamental mechanisms of redox reactions on the crystal surface of TiO_2 will be beneficial for designing new photocatalysts for application in the fields of energy and environment. For a long time period, researches have focused on the methodology for improving the photocatalytic efficiency of TiO_2, such as metal and nonmetal doping and compositions of different materials. The combination of noble-metal nanostructures and semiconductor may provide a way for enhanced catalytic applications.[1,7,8]

Photocatalytic efficiency can be improved by depositing noble metals on the TiO_2 surface for photogenerated electrons trapped in the noble metals to reduce the electron−hole recombination rate.[9,10] The photogenerated electrons transfer to the metal particles when they are in contact with TiO_2, so that the Fermi level (E_F) of the noble metal becomes more negative until reaching the equilibrium between the E_F and conduction band.[9] In addition to the electron trap mechanism, plasma-excited high-energy electrons from the noble-metal nanoparticle flow to the TiO_2 to promote electron−hole separation, and then the electron−hole pairs can be used in the photocatalytic reactions.[11] The surface plasmon resonance (SPR) effect[12] caused by visible light irradiation can enhance the photocatalyst performance. Recently, SPR of Au nanoparticles has been applied to a visible light-responding photocatalyst.[13−17] SPR photoabsorption by Au particles is found to be one of the important factors governing the rate of the H_2 evolution.[12] The separation of photogenerated electron−hole pairs via localized SPR is greatly enhanced, and the activity of $Au−TiO_2$ for both photocatalytic hydrogen evolution and methylene blue decomposition could be promoted and obtained under visible light irradiation.[18] In addition to forming a composite material coupled with Au and

Received: July 9, 2015
Accepted: August 26, 2015
Published: August 26, 2015

DOI: 10.1021/acsami.5b06161
ACS Appl. Mater. Interfaces 2015, 7, 20349−20359

Ag nanoparticles, Pt as an electron sink deposited on TiO_2 also substantially enhances the separation of photogenerated electron−hole pairs for photocatalytic degradation organic pollutants.[19−21] The loaded Pt with a large work function induces the formation of a Schottky barrier in the TiO_2−metal region and assists the interfacial multielectron transfer.[22] Thus, the migration of photogenerated electrons from the TiO_2 conduction band (CB) to the metal phase retards the recombination of electron−hole pairs and subsequently increases the photocatalytic activity. Moreover, the electron-sink function of Pt coupled with the Au SPR effect could synergistically enhance the photocatalytic activity.[23] The higher overall activity of the Pt-loaded TiO_2 catalyst is attributed to the more effective trapping and pooling of photogenerated electrons on Pt and/or to the higher intrinsic platinum activity in both hydrogen production and complete methanol oxidation.[24]

Anatase TiO_2 nanostructures usually exhibit superior performance over the rutile counterparts in photoelectrochemical systems, due to the facile charge transport and efficient separation of light-induced electron−hole pairs.[25−27] However, the formation of anatase nanostructures usually involves complex and laborious steps. Catalytic reactions occur at the surface of TiO_2, and thus, catalytic activity is largely dependent upon crystalline structure and exposed facets.[28,29] Anatase (001) planes with a high surface energy of 0.90 J/m^2 usually vanish rapidly in the crystal growth[30] until an anatase TiO_2 single crystal containing 47% of (001) facets was first synthesized.[25] The anatase (101) plane is the most stable surface with the lowest surface energy of 0.43 J/m^2.[31] Surface-dependent photocatalytic activity of anatase TiO_2 nanocrystals could be systematically evaluated by preparing TiO_2 with different exposed surfaces. For example, the photodegradation efficiency of anatase TiO_2 toward methylene blue over (001) planes is superior to that over (101) planes,[32] but the photocatalytic activity of the (101) surface is higher than that of the (001) surface for the selective conversion of glycerol to hydroxyacetaldehyde in aqueous solution.[33] These contradictory results remind us that the photocatalytic performance of the crystal surface of anatase may be affected not only by the surface energy but also by the target contaminants.[34] The most common morphology for surface-dependent activity is truncated tetragonal bipyramidal anatase crystals with coexisting (001) and (101) planes.[31]

Although previous studies have shown the facet-dependent performance of TiO_2 in the photocatalytic reactions,[35−38] information regarding the noble-metal-loaded TiO_2 for its facet-dependent photocatalytic performance, particularly in the case of pollutant degradation systems, is still limited. Meanwhile, the photocatalytic degradation of nitrobenzene (NB) by nanocrystalline TiO_2 has been investigated by various groups.[39−41] For instance, the NB degradation efficiency of nanocrystalline TiO_2 was found to be improved by loading graphitic carbon[39] and coating dihydroxynaphthalene onto Pt/TiO_2.[41] Besides, surface modification of TiO_2 was reported to be able to improve selective pollutant conversion[42] and facilitate the interaction with the desired target contaminants.[43,44] In the case of Pt nanoparticles selectively loaded on the (101) facets under irradiation, both photocatalytic hydrogen evolution (photoreduction) and photocatalytic degradation of methyl orange (photooxidation) processes could be enhanced.[45] The highest phenol degradation efficiency could be achieved with Pt nanoparticles deposited on the (101) and (010) facets.[46] However, for the process of oxidation of formaldehyde into CO_2, the photocatalytic activity of the dominant surface has not been provided for the Pt/TiO_2 photocatalyst.[47] Thus, more studies are needed to explore the photoreduction and photooxidation activities of the facets for the target contaminants. Understanding the surface−performance relationship with noble metal loaded at the atomic level will provide theoretical guidelines for improving the photocatalytic activity of anatase TiO_2 crystals in practical applications. In addition, the performance of superstructure systems with well-regulated morphologies can be improved by exploring the crystal-facet-dependent photocatalytic reactions.[48] A systematic study of the degradation mechanisms for different pollutants on a specific surface could provide a superior surface environment for enhancing the photocatalytic efficiency and lowering the cost, which are beneficial for large-scale applications.

In a previous study,[49] we conducted first-principles theoretical calculations about the roles of the crystal surface in Pt-loaded TiO_2 in its photocatalytic capacity and found that the (001) facets of TiO_2 in this complex tended to accumulate more positively charged holes and thus have a higher photocatalytic activity than the (101) facets. Inspired by these informative results, in this study, we aimed to explore the facet-dependent mechanism of the Pt cluster-loaded nanocrystalline TiO_2 (Pt/TiO_2) composite catalyst for the degradation of nitrobenzene (NB), which has been widely used as a model pollutant to evaluate the photocatalytic activity of designed catalysts.[50,51] Anatase TiO_2 nanocrystals with an interspersed polyhedron morphology and coexposed (001) and (101) facets were prepared with a Ti source and morphology controlling agent of NH_4F. The formation mechanism of this polyhedron structure was investigated. TiO_2 nanocrystals with different crystal planes exposed as a support of Pt nanoparticles were prepared to examine the effect of the crystal face on the NB degradation efficiency on Pt/TiO_2 catalysts. The crystal morphologies of Pt nanoparticles supported on different TiO_2 crystal planes were also investigated to provide new insights for designing effective goal-targeted noble-metal-loaded photocatalysts.

EXPERIMENTAL SECTION

Preparation of the Pt Cluster-Loaded TiO_2. Nanocrystalline TiO_2 was synthesized using 40 mL of HCl (6 mol/L) and 0.4 g of Ti foil via a hydrothermal method. Ammonium fluoride (NH_4F) (0.15 g) dissolved in 15 mL of the as-prepared solution was added into a 50 mL beaker. After that, the mixed solution was stirred for 15 min, 5 mL of water was added, and the mixture was further stirred for 15 min and transferred into a 50 mL polytetrafluoroethylene-lined stainless autoclave. The hydrothermal synthesis was conducted in an electric oven at 160 °C for 12 h. After the reaction was completed, the autoclave was cooled to room temperature. Then, the obtained samples were ultrasonically washed with ethanol and deionized water in sequence. Before the photocatalytic characterization, all the hybrid samples were rinsed with NaOH (0.1 M) and deionized water to remove the adsorbed fluorine ions. All chemicals used in this work were analytical-grade reagents and used without further purification.

Pt nanoparticles (1 wt %) were simultaneously deposited on the (001) and (101) surfaces of TiO_2 catalysts by chemical deposition. Pt nanoparticles (1 wt %) were only deposited on the (101) surface of TiO_2 catalysts by photoreduction. The deposition process was as follows: First, 0.2 g of TiO_2 powder, 100 mL of ethanol, $H_2PtCl_6 \cdot 6H_2O$ (2 mg Pt), and 50 mg of ascorbic acid were added sequentially to a three-neck flask. Then, the suspension was mixed under heating reflux and constant stirring. After 1 h deposition, gray-colored powders

DOI: 10.1021/acsami.5b06161
ACS Appl. Mater. Interfaces 2015, 7, 20349−20359

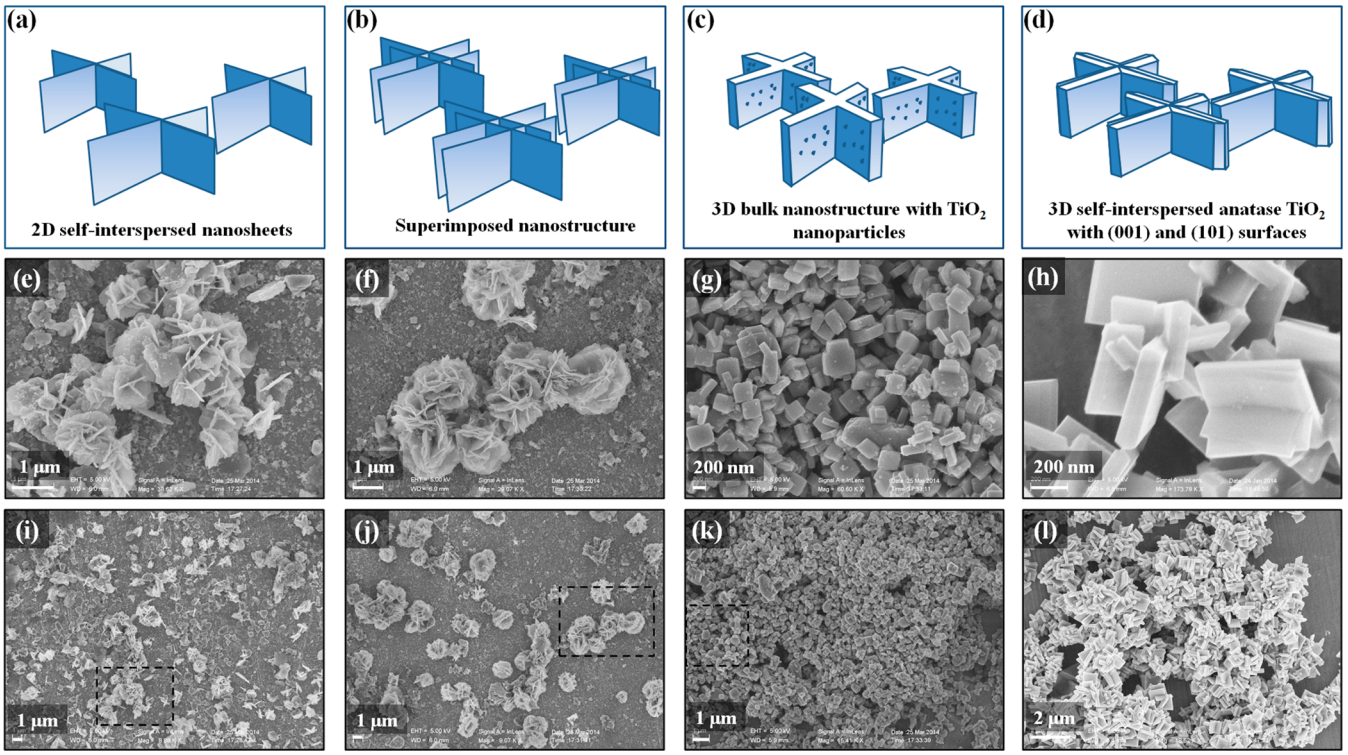

Figure 1. Proposed formation mechanism of 3D self-interspersed anatase TiO_2 (a–d). (a) 2D self-interspersed nanosheet formed for 1.5 h hydrothermal synthesis at 160 °C with the corresponding SEM images (e) and the wide range image (i). (b, f, j) Assembled nanostructure from (a) after 2 h. (c, g, k) 3D bulk nanostructure fabricated from (b) with the TiO_2 nanoparticles on the surface after 3 h. (d, h, l) 3D self-interspersed anatase TiO_2 composed with the exposed surfaces of (001) and (101) after 12 h.

were obtained, which were centrifuged, dried at 60 °C for 1 h, and then annealed at 450 °C in air for 1 h.

Characterization. Scanning electron microscopy (SEM) imaging of the samples was performed on a Zeiss Supra 40 field emission scanning electron microscope at an acceleration voltage of 5 kV. Transmission electron microscopy (TEM) images, high-resolution (HR) TEM images, and selected-area electron diffraction (SAED) patterns of Pt/TiO_2 nanocrystals were obtained on a transmission electron microscope (JEM-2010, JEOL Co., Japan) with an accelerating voltage of 200 kV. Powder X-ray diffraction (XRD) patterns were obtained using a MXPAHF diffractometer (MacScience Co., Japan) with a Cu Kα radiation source (λ = 1.54056 Å). The scanning speed was set at 8°/min to determine the crystal phase of the samples. The accelerating voltage and the applied current were 30 kV and 300 mA, respectively. The Pt element in the Pt-loaded TiO_2 samples was determined by using inductively coupled plasma atomic emission spectrometry (ICP-AES) (Optima 7300 DV, PerkinElmer Inc., USA). The measurement of surface area was conducted using the Brunauer–Emmett–Teller (BET) method at −195.8 °C on a TriStar II 3020 V1.03 (Micromeritics Instrument Co., USA). The chemical compositions and the valence states of constituent elements were analyzed by X-ray photoelectron spectroscopy (XPS) (ESCALAB250, Thermo Fisher Inc., USA). Ultraviolet–visible (UV–vis) absorption spectra analysis of the samples was conducted with a UV–vis spectrophotometer (SOLID3700, Shimadzu Co., Japan). The photoluminescence (PL) measurement of the samples was carried out with a photoluminescence spectrophotometer (5301, Shimadzu Co., Japan).

Photocatalytic Degradation of NB on Pt/TiO_2. A Xe lamp (CHF-XM-350W, Beijing Trusttech. Co., China) was used as the light source for the photocatalytic degradation experiment. UV (λ < 420 nm) or visible light ($\lambda \geq$ 420 nm) irradiation was selectively applied by utilizing a visible (UV) cut filter. Before the experiment, 1 mg/mL of the synthesized catalyst was transferred into 25 mL of the reaction solution. The initial NB concentration was 10 mg/L. The photocatalytic reaction was initiated by using the irradiation generated from a 15 A external current. In the photodegradation, the solution was sampled every 10 min for analyzing the concentration changes of NB and its degradation products. The total organic carbon (TOC) concentrations of the samples were measured using a TOC analyzer (multi N/C 2100, Analytik Inc., Germany) to confirm the mineralization of NB. The intensities of the visible light source (in mW/cm^2) and the UV light source (in mJ/cm^2) were measured using a radiometer (Model FZ-A, Photoelectric Instrument Co., China) and a UV-integrator (KÜHNAST Inc., Germany), respectively. The photoconversion efficiency (ε_{eff}) can be expressed as a function of photocurrent density in the presence of an externally applied potential. The NB concentration was determined using high-performance liquid chromatography (HPLC-1100, Agilent Inc., USA) equipped with a Hypersil-ODS reversed-phase column and a VWD detector. The mobile phase was a 0.1% acetic acid and methanol (40:60) water solution delivered at a flow rate of 0.8 mL/min. The NB degradation products were analyzed by liquid chromatography mass spectrometry (LC/MS, Agilent 6460).

Photocurrent Intensity Measurement. The photocurrent intensity was recorded on a CHI 760D electrochemical workstation (Shanghai Chenhua Co., China) with a three-electrode system. In the system, a photocatalyst (0.1 mg dispersed in 0.1 mL of aqueous solution), a modified fluorine-doped tin oxide (FTO) electrode (1.5 cm × 3.0 cm) was used as the working electrode, a Pt wire was used as the counter electrode, and a Ag/AgCl electrode was used as the reference electrode. All the photocurrent measurements were carried out in Na_2SO_4 solution (0.1 M, pH 7.0), and the applied potential (E_{app}) was 0.1 V (versus Ag/AgCl, i.e., 0.3 V versus SHE).

$$E_{app} = E_{meas} - E_{aoc} \quad (1)$$

where E_{meas} is the electrode potential with respect to a reference electrode at which photocurrent is measured and E_{aoc} is the electrode potential at open circuit under the same conditions.[52]

DOI: 10.1021/acsami.5b06161
ACS Appl. Mater. Interfaces 2015, 7, 20349–20359

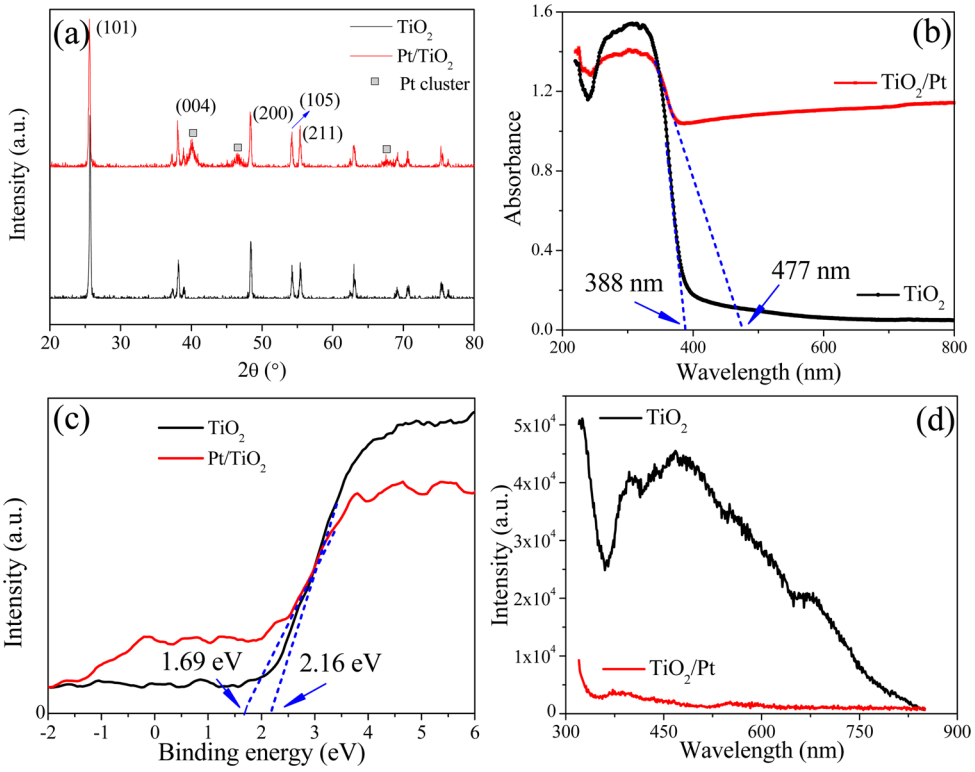

Figure 2. (a) XRD patterns, (b) UV−vis diffuse reflectance spectra, (c) XPS valence band spectra, and (d) PL spectra of pure TiO_2 and Pt/TiO_2 samples.

RESULTS AND DISCUSSION

Formation Mechanism of Self-Interspersed Anatase TiO_2. Anatase TiO_2 is a truncated octahedral bipyramid comprising of eight (101) facets on sides and two (001) facets on the top and bottom.[25,31] Figure 1 shows the proposed formation mechanism of the self-interspersed nanostructure with the corresponding SEM images of the intermediate states and the obtained anatase TiO_2 nanocrystals, whereas Figure 1i−l illustrates the wide range images. As shown in Figure 1e, the 2D self-interspersed TiO_2 nanosheets were formed in the hydrothermal process after 1.5 h at the initial stage. Then, the 2D interspersed nanosheets continued to superimpose on each other and formed a more complex interspersed architecture (Figure 1b,f,j). After 3 h of hydrothermal synthesis, 3D bulk nanostructures were obtained with small TiO_2 nanoparticles on the surfaces (Figure 1c,g,k). Finally, a self-assembled 3D anatase TiO_2 architecture were formed with a large percentage of smooth (001) surfaces after 12 h of hydrothermal synthesis. A thermodynamic model based on surface free energies and surface tensions can be used to evaluate the effects of surface chemistry on the morphology and phase stability of anatase nanocrystals.[53,54] Then, the target morphology and the exposed surfaces of the anatase architecture could be tailored in the synthesis. Moreover, the polyhedral 3D self-interspersed structures demonstrate the unique synergistic properties and compose the pore space between self-assembled TiO_2 nanocrystals to accelerate the diffusion of reactants and products for the improved photocatalytic capacity.[55,56]

The fluorine ion (F^-) plays an important role in the synthesis of anatase crystals with dominant (001) facets since the first demonstration by Yang et al.[25] The high F−Ti bonding energy significantly lowers the energy of the (001) surfaces.[57] In the traditional method, F^- is contributed by the crystallographic controlling agent, i.e., hydrofluoric acid (HF). However, NH_4F was used in this work as the capping agent to control the exposed surface so as to avoid use of the highly corrosive liquid, i.e., HF. Meanwhile, NH_4^+ might provide the opportunity of forming the interspersed nanostructures because of the steric effect and the electrostatic attraction with F^-. NH_4^+ could be self-assembled on the TiO_2 surface to form the surface electric dipole moment.[58] The roles of NH_4^+ in such a synthesis warrant further investigations.

Microstructure of the Pt/TiO_2 Photocatalyst. The as-prepared TiO_2 samples were subjected to XRD analysis, which confirms the formation of anatase TiO_2 (JCPDS 21-1272) (Figure 2a). Here, the diffraction peaks at 25.32, 37.93, 48.02, 53.98, and 55.04° correspond to the (101), (004), (200), (105), and (211) planes of anatase TiO_2, respectively. In addition, the diffraction peaks of the Pt/TiO_2 composite reveal that the photodeposited Pt had a cubic phase (JCPDS 4-802).

SEM and TEM images indicate that the TiO_2 particle was decahedral in shape with (001) and (101) exposed crystal faces (Figure 3). The Pt nanoparticles derived from the chemical reduction preparation processes exhibit uniform distributions on the TiO_2 facets (Figure 3c). HRTEM was used to directly observe the location of Pt clusters on the nanocrystalline TiO_2. The HRTEM images of a single TiO_2 nanocrystal show a lattice spacing of 0.19 nm (Figure 3d), which matches well the interplanar spacing of the (020) and (200) plane of decahedral TiO_2. The SAED patterns (inset of Figure 3d) further confirm that anatase nanocrystallites were indeed formed and the angle between (200), zero point, and (020) was 90°. In addition, the lattice spacing observed here is in good agreement with the XRD results. Furthermore, photodeposited Pt nanoparticles were uniform in size and existed in the different crystal faces of the TiO_2 nanocrystal, including (001) and (101) surfaces. The

DOI: 10.1021/acsami.5b06161
ACS Appl. Mater. Interfaces 2015, 7, 20349−20359

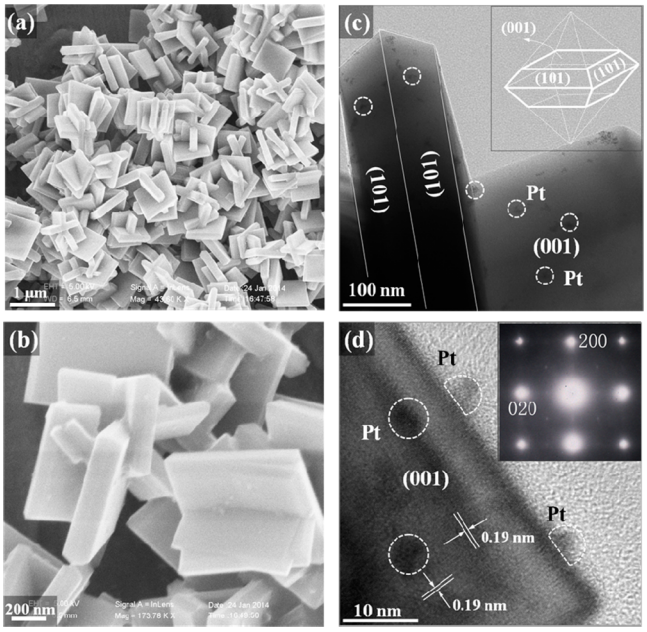

Figure 3. (a) SEM images of bare TiO_2 nanocrystals with the morphology of the nanocrystalline anatase TiO_2 from the hydrothermal synthesis with a scale bar of 1 μm and (b) with a scale bar of 200 nm. (c) TEM and (d) HRTEM images of Pt/TiO_2 samples with (001) and (101) surfaces. Inset of (c): schematic illustration of the crystal orientation. Inset of (d): SAED pattern of anatase TiO_2.

ICP-AES analysis shows that the total Pt content loaded on these two exposing surfaces was 11.77 μg/mL.

The BET specific surface area and the corresponding pore-size distribution of the synthesized anatase and Pt-loaded TiO_2 were evaluated using the BET method (Figure 4). According to Brunauer–Deming–Deming–Teller (BDDT) classification,[59,60] the isotherms belong to Type IV with an H3 hysteresis loop, which are typical for mesoporous materials. The SEM and TEM images indicate that these mesopores were related to the space between the aggregated nanocrystals because of the absence of a pore structure inside the individual nanopcrystals. The BET surface areas of the anatase TiO_2 and Pt/TiO_2 calculated from the N_2 adsorption results were 5.9 and 6.6 m^2/g, respectively. The Pt-loaded TiO_2 polyhedron nanostructures with higher specific surface areas are beneficial for promoting photocatalytic activity by facilitating the absorption of pollutants for degradation.

The XPS analysis was performed to explore the surface compositions and the binding energy of the as-prepared Pt-loaded TiO_2 nanocrystals (Figure 5). As shown in Figure 5a, the survey spectrum contains the peaks of O, Ti, and Pt elements, indicating the surface constitution of the hybrid nanostructure of Pt/TiO_2. The C 1s peak observed in the survey comes from the background. The Ti 2p XPS spectrum (Figure 5b) shows two main peaks with binding energies at 458.5 and 464.2 eV, corresponding to Ti $2p_{3/2}$ and Ti $2p_{1/2}$, respectively. The O 1s XPS spectrum (Figure 5c) could be fitted well with the peak at 529.7 eV, which belongs to O^{2-} from the Ti–O bond on the surface atomic structures of the host TiO_2 for noble-metal loading. The Pt/TiO_2 photocatalyst presents two obvious peaks of Pt $4f_{7/2}$ and $4f_{5/2}$ at 70.3 and 73.6 eV (with the splitting energy Δ = 3.3 eV, Figure 5d), respectively, indicating the existence of the metallic Pt.[61]

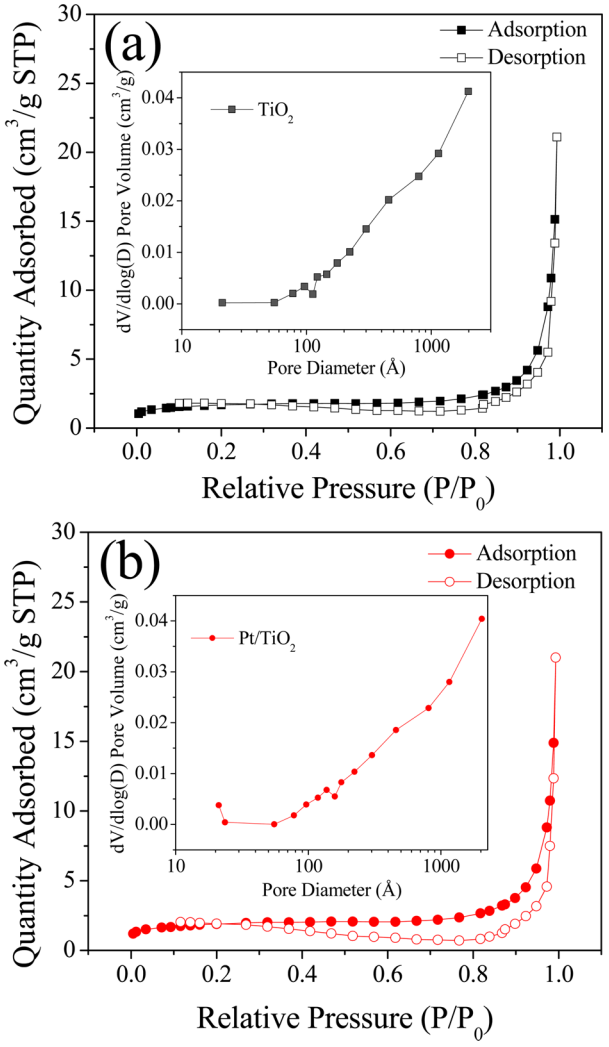

Figure 4. Nitrogen adsorption–desorption isotherm plot and corresponding pore-size distribution (inset) of the as-prepared anatase TiO_2 and Pt/TiO_2.

An enhanced visible light adsorption of the TiO_2 nanocrystals induced by Pt nanoparticles was also evidenced by the UV–vis diffusion reflectance spectra (DRS) of the photocatalysts (Figure 2b). The Pt/TiO_2 composite exhibited a significantly higher absorption in the visible region than the bare TiO_2 nanocrystal, attributed to the electron sink effect of the Pt nanoparticles.[12] The optical band gap of a phototcatalyst can be calculated with the following equation[62]

$$\alpha(h\nu) = A(h\nu - E_g)^{n/2} \quad (2)$$

where α is the absorption coefficient, $h\nu$ is the photon energy, E_g is the optical band gap, n is assumed to be 1 for the direct transition type (n = 4 for the indirect transition), and A is a constant concerning the transition probability.

The absorption edges of TiO_2 and Pt/TiO_2 were located at 388 and 477 nm (Figure 2b), and the wavelength data could be transformed into their band gap values of 3.2 and 2.6 eV, respectively.[63,64] The valence band (VB) of each sample measured by XPS VB spectra is shown in Figure 2c. The VB edge of Pt/TiO_2 (1.69 eV) below the Fermi energy indicates that the Pt loading causes a slight shift of the VB location to the lower energy level. Moreover, the conduction band (CB) of Pt/

DOI: 10.1021/acsami.5b06161
ACS Appl. Mater. Interfaces 2015, 7, 20349–20359

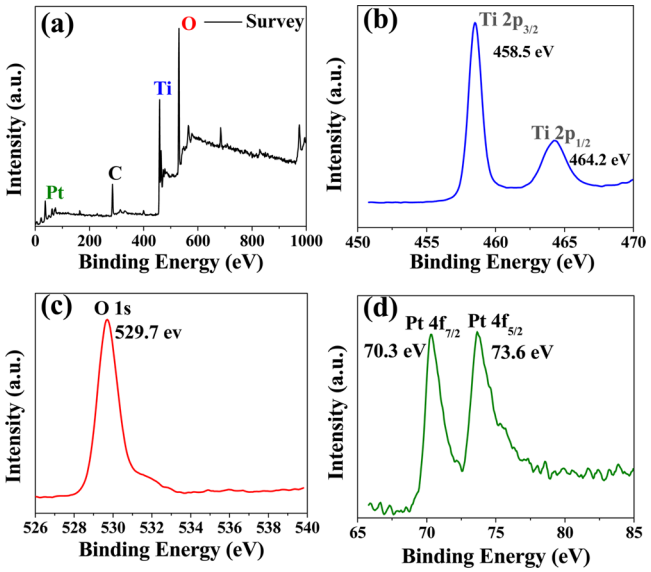

Figure 5. XPS spectra of Pt-loaded TiO_2 nanocrystals: (a) survey spectrum, (b) Ti 2p spectral region, (c) O 1s spectral region, and (d) Pt 4f spectral region.

TiO_2 (−0.91 eV, $E_g = E_{VB} - E_{CB}$) locates closer to the Fermi energy than the TiO_2 polyhedron nanostructures. These results indicate that the Pt/TiO_2 had a narrower band gap in the visible light region, which is in agreement with the previous reports[65,66] and our theoretical predictions.[49] Such a polyhedron structure with Pt loading on both the (001) and the (101) surfaces might facilitate the separation of photoexcited electrons and holes and could substantially enhance the photocatalytic activity.

On the other hand, the fluorescence spectra of the photocatalysts imply that Pt loading decreased the recombination of electron−hole pairs. As shown in Figure 2d, the Pt/TiO_2 showed a much lower PL intensity than the bare TiO_2 in the wavelength range of 300−850 nm. Since PL is the emission of fluorescence originating from the recombination of photogenerated electron−hole pairs, the decreased PL intensity of the Pt/TiO_2 indicates a lower density of recombination centers and, consequently, higher availability of effective photogenerated carriers for catalytic reactions. Such a decreased electron−hole recombination might be ascribed to an accelerated transfer of the photogenerated electrons from the CB of TiO_2 to the Pt cluster.

Application of Pt/TiO_2 and Photoconversion Efficiency. To examine the roles of Pt nanoparticles, the photocatalytic degradation of NB on both bare and Pt-loaded nanocrystalline TiO_2 was investigated, and these processes were repeated three times. The incident visible light intensity ($I_{0,vis}$) was about 160 mW/cm^2, and the UV light intensity ($I_{0,UV}$) showed 157 mJ/cm^2 for 60 s, i.e., 2.6 mW/cm^2. Figure 6a,b illustrates the NB photodegradation process over time, which follows the first-order kinetics. Therefore, the apparent degradation rate constant (k) of NB could be obtained from the slope of the $\ln(C/C_0)$ versus time fitting line, in which C represents the NB concentration. Each error bar indicates the

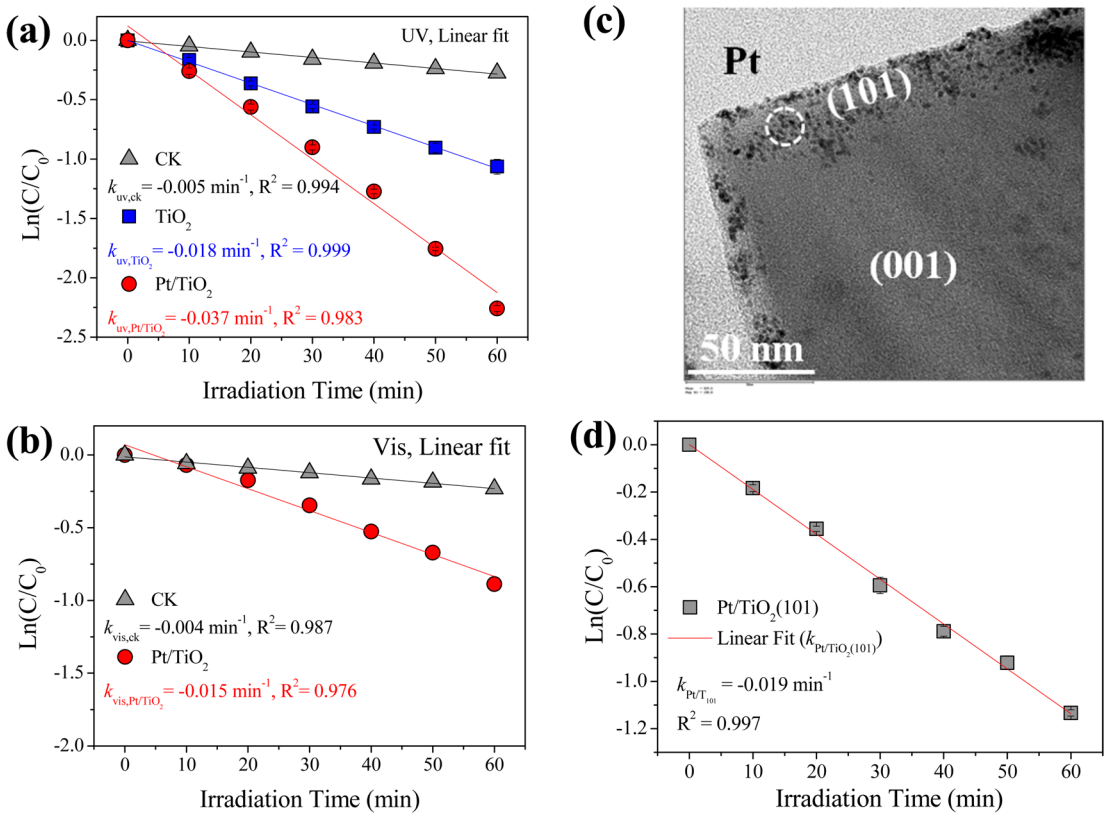

Figure 6. Photocatalytic degradation of NB in aqueous solution under UV ($I_{0,UV}$ = 2.6 mW/cm^2) irradiation, in the presence of no photocatalyst (CK), bare TiO_2, and Pt/TiO_2 (a), and visible light ($I_{0,vis}$ = 160 mW/cm^2) irradiation, in the presence of no photocatalyst (CK) and Pt/TiO_2 (b). (c) TEM image of Pt/TiO_2(101) samples and (d) photocatalytic degradation of NB in aqueous solution under UV light irradiation ($I_{0,UV}$ = 2.6 mW/cm^2), in the presence of Pt/TiO_2(101) as photocatalyst. Here, C_0 and C refer to the NB concentrations at t = 0 and t = t, respectively.

DOI: 10.1021/acsami.5b06161
ACS Appl. Mater. Interfaces 2015, 7, 20349−20359

standard deviation. The detailed statistic results of the NB photocatalytic degradation kinetic data are given in Table 1. A

Table 1. Kinetic Constants and Regression Coefficients of Photocatalytic NB Degradation under Visible and UV Light Illumination

		slope kinetic constant (min^{-1})		statistics
light source	photocatalyst	value	standard error	R^2
vis	Pt/TiO_2	−0.015	0.00095	0.976
UV	TiO_2	−0.018	0.00025	0.999
	Pt/TiO_2	−0.037	0.00203	0.983
UV	$Pt/TiO_2(101)$	−0.019	0.00045	0.997

comparison of the NB degradation rate constants with different catalysts shows that the fastest NB degradation was achieved by the Pt/TiO_2 under UV irradiation. The k_{Pt/TiO_2} was 2 times larger than the k_{TiO_2} in absolute value under UV light radiation. In addition, the overall removal efficiency of NB within 1 h of UV irradiation in the Pt/TiO_2 system was higher than that in the TiO_2 system by 30%. All of these results confirm that the Pt cluster led to a significantly improved NB photodegradation. Notably, a slow decrease in NB concentration in the absence of any photocatalyst was also observed, possibly due to a direct photodegradation in this system. A similar slow degradation of pollutants in the absence of catalysts was also observed by others.[39] Moreover, TOC removal efficiency was used to evaluate the mineralization of the NB in the photocatalytic oxidation with different photocatalysts. The TOC removal efficiency of Pt/TiO_2 reached 55% after 1 h of irradiation, higher than that (46%) for TiO_2. The results indicate that Pt/TiO_2 possesses a higher mineralizing ability, mainly due to the promotion in separation of electrons and holes by loading Pt nanoparticles.

The photoconversion efficiency (ε_{eff}) reflects the average value of quantum efficiency (QE) at different wavelengths,[52,67] QE of semiconductors, which measures the absolute yield within a material from exciton creation to photon emission, and is inherently tied to the photonic and optoelectronic properties. The ε_{eff} in the presence of an externally applied potential (E_{app}) can be expressed as follows[46,52]

$$\varepsilon_{eff} = j_p(E^{\ominus}_{rev} - |E_{app}|)/I_0 \quad (3)$$

where j_p is the photocurrent density ($\mu A/cm^2$), $E^{\ominus}_{rev}$ is the thermodynamic standard state reversible potential when the reaction occurs, I_0 is the intensity (power density, mW/cm^2), and the $|E_{app}|$ is the absolute value of the applied potential. Here, the water splitting reaction ($E^{\ominus}_{rev}$ = 1.23 V) was used to measure the ε_{eff} of the photocatalysts under UV or visible light irradiation.

To further investigate the photoresponse, the photocurrent over time was measured under UV (2.6 mW/cm^2) and visible light (160 mW/cm^2) illumination (Figure 7) with a light on/off circle of 100 s and an E_{app} of 0.3 V (vs SHE). Thus, the ratio of $\varepsilon_{eff,Pt/TiO_2}/\varepsilon_{eff,TiO_2}$ under UV light was about 1.3, and the ratio of $\varepsilon_{eff,Pt/TiO_2,UV}/\varepsilon_{eff,Pt/TiO_2,vis}$ was approaching 600. The details for photoconversion efficiency ratio calculations are provided as follows.

The ratio of $\varepsilon_{eff,Pt/TiO_2}/\varepsilon_{eff,TiO_2}$ with the same intensity of incident light could be expressed as

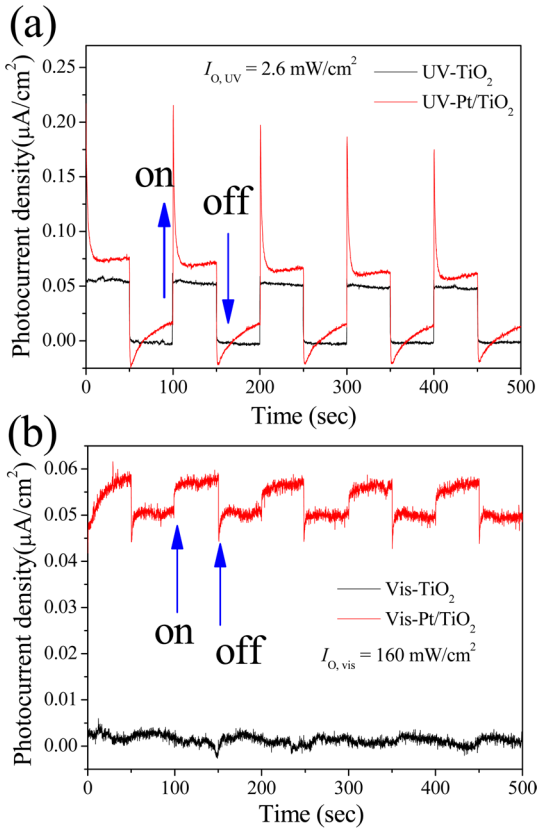

Figure 7. Photocurrent responses of the as-prepared bare-TiO_2/FTO and Pt/TiO_2/FTO electrode under UV ($I_{0,UV}$ = 2.6 mW/cm^2) (a) and vis ($I_{0,vis}$ = 160 mW/cm^2) (b) irradiation in 0.1 M Na_2SO_4 solution recorded at an applied potential (E_{app}) of 0.3 V (versus SHE); the light on/off cycle is 100 s.

$$\frac{\varepsilon_{eff,Pt/TiO_2}}{\varepsilon_{eff,TiO_2}} = \frac{j_{p,Pt/TiO_2}}{j_{p,TiO_2}} \quad (4)$$

The value of $j_{p,Pt/TiO_2}$ under UV light is (0.0657 ± 0.0063) $\mu A/cm^2$, and the j_{p,TiO_2} is (0.0521 ± 0.0027) $\mu A/cm^2$ (Figure 7a). Thus, the value of $\varepsilon_{eff,Pt/TiO_2}/\varepsilon_{eff,TiO_2}$ is 1.3 with the incident light intensity of 2.6 mW/cm^2.

The ratio of $\varepsilon_{eff,Pt/TiO_2,UV}/\varepsilon_{eff,Pt/TiO_2,vis}$ with different intensities of incident light can be expressed as

$$\frac{\varepsilon_{eff,Pt/TiO_2,UV}}{\varepsilon_{eff,Pt/TiO_2,vis}} = \frac{j_{p,Pt/TiO_2,UV}\cdot I_{0,vis}}{j_{p,Pt/TiO_2,vis}\cdot I_{0,UV}} \quad (5)$$

The value of $j_{p,Pt/TiO_2}$ under visible light (160 mW/cm^2) is (0.0068 ± 0.0002) $\mu A/cm^2$. Thus, the value of $\varepsilon_{eff,Pt/TiO_2,UV}/\varepsilon_{eff,Pt/TiO_2,vis}$ is calculated to be 591.

These results confirm that the decreased PL intensity of Pt/TiO_2, and the metallic units might enhance the photocatalytic efficiency by promoting charge separation at the metal−semiconductor interfaces.[13] The Pt particles, because of their better electron affinity than TiO_2, could serve as an electron sink to reserve the photogenerated electrons from TiO_2, and hence prevent the electron−hole recombination, and finally promote the photocatalytic efficiency.

Photocatalytic NB Conversion Mechanisms on Different Crystal Surfaces of Pt/TiO_2. To better understand the

DOI: 10.1021/acsami.5b06161
ACS Appl. Mater. Interfaces 2015, 7, 20349−20359

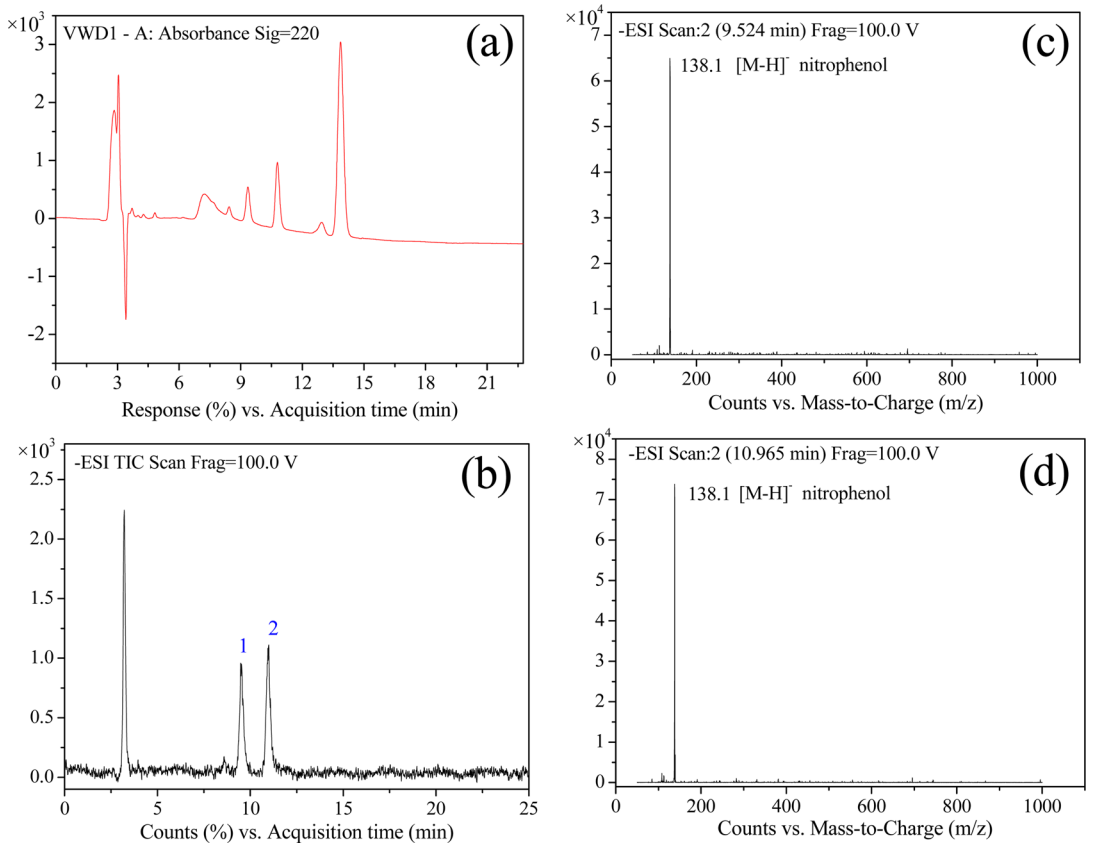

Figure 8. LC/MS chromatograms of the photocatalytic degradation intermediates of NB on Pt/TiO_2: (a) UV spectra, (b) LC, (c) MS of intermediate product 1 at 9.524 min, and (d) MS of intermediate product 2 at 10.965 min. $[M - H]^-$ = 138; the intermediate products may be *o*-nitrophenol, *m*-nitrophenol, and *p*-nitrophenol. The substance at 3.208 min is an impurity. LC/MS conditions: column, Zic-HILIC (150 mm × 2.0 mm i.d.); flow rate, 0.2 mL/min; mobile phase, methanol/0.05% formic acid = 50/50; temperature, 30 °C; injection, 1.0 μL; and detection, MS-ESI - *m*/*z* (10−300).

mechanism of NB phototcatalytic conversion on the Pt/TiO_2, the intermediate products were analyzed by LC/MS (Figure 8). After 1 h of illumination, the concentration of NB decreased by 90%, but only nitrophenol intermediates were detected by LC/MS, indicating that the degradation proceeded via $^{\bullet}OH$ oxidation. $^{\bullet}OH$ could be generated from the hydroxyl groups in aqueous solution at the positive holes (h_{VB}^+) formed on the valence band (VB). According to the previous studies,[68] the intermediates of NB degradation in the reduction pathway included nitrosobenzene (NSB) and hydroxylaminobenzene (HAB), and the product was aniline. Moreover, the photocatalytic oxidation of NB degradation was mainly through generating $^{\bullet}OH$ radicals.[68] Furthermore, the (001) facets of anatase TiO_2 are the photooxidative sites, whereas the (101) facets are the reductive sites in photocatalytic reactions.[69] The reduction and oxidation reactions are spatially separated on different facets of TiO_2. This indicates that the NB degradation might proceed through a photooxidation pathway on the (001) surface of Pt/TiO_2, which is in agreement with the theoretical prediction in our previous work.[49]

To validate the above results, the photocatalytic degradation of NB on the $Pt/TiO_2(101)$ was investigated. $Pt/TiO_2(101)$ was synthesized by photoreduction, in which Pt nanoparticles (1 wt %) were selectively deposited on the (101) surface of TiO_2 catalysts (Figure 6c). The total Pt content loaded on the (001) and (101) surfaces was 11.77 μg/mL, whereas the Pt content of the $Pt/TiO_2(101)$ was 11.97 μg/mL, which was almost the same as the Pt content value in the sample Pt/TiO_2. Thus, the influence of the Pt loading amount on the photocatalytic performance could be neglected. Figure 6d illustrates the NB photodegradation process over time on the $Pt/TiO_2(101)$, which also follows the first-order kinetics. Table 1 shows the detailed statistical results of the photocatalytic kinetic data of the $Pt/TiO_2(101)$. Thus, the apparent NB degradation rate constant (k) could be obtained. The $k_{Pt/TiO_2(101)}$ was only half of the k_{Pt/TiO_2} (Figure 6a) in absolute value under UV light radiation. In addition, the overall NB removal efficiency on the $Pt/TiO_2(101)$ within 1 h of UV irradiation was of almost the same level with that on TiO_2, and lower than that on the Pt/TiO_2. Therefore, the Pt cluster only deposited on the (101) surface had no significant effect on the improvement of NB photodegradation. This further suggests that the NB photodegradation is favored in the direction of the oxidation pathway on the Pt cluster-loaded (001) surface of anatase TiO_2.

CONCLUSIONS

In this work, a simple and green strategy for the synthesis of high (001) facet exposed anatase TiO_2 nanocrystals with an interspersed polyhedron morphology is developed, and Pt nanoparticles uniformly dispersed on both of the (001) and (101) facets are successfully prepared by using a chemical reduction deposition approach. In this way, the efficient photocatalytic degradation of the model pollutant, NB, could be achieved by taking advantage of the crystal surface of Pt/

DOI: 10.1021/acsami.5b06161
ACS Appl. Mater. Interfaces 2015, 7, 20349−20359

TiO_2 with a high photocatalytic activity. Uniformly loading Pt nanoparticles on the crystal surfaces substantially enhances the NB photodegradation efficiency, but the Pt nanoparticles deposited on the (101) surface only have no contribution to the improved NB photodegradation. The NB degradation on Pt/TiO_2 proceeds via photocatalytic oxidation on the (001) surface through generating $^{\bullet}OH$ radicals. The (001) surface loaded with Pt nanoparticles has a considerable contribution to the enhanced NB degradation. Thus, exposing a large ratio of the (001) surface in the synthesis of Pt/TiO_2 could improve the photocatalytic NB degradation efficiency. Our work provides new insights into designing contaminant-targeted noble-metal-loaded photocatalysts with an appropriate crystal surface and might deliver useful information for guiding synthetic strategies in other noble-metal nanoparticles and bimetallic nanostructures deposited on semiconductor supports for various catalytic applications.

AUTHOR INFORMATION

Corresponding Author

*Fax: +86 551 63601592. E-mail: hqyu@ustc.edu.cn.

Author Contributions

†These authors contributed equally.

Notes

The authors declare no competing financial interest.

ACKNOWLEDGMENTS

The authors wish to thank the National Basic Research Program of China (2011CB933702), the National Natural Science Foundation of China (51538011), the Program for Changjiang Scholars and Innovative Research Team in University and the Collaborative Innovation Center of Suzhou Nano Science and Technology of Ministry of Education of China, and the China Postdoctoral Science Foundation (2014M560522) for the partial support of this work. The numerical calculations were performed on the supercomputing system in the Supercomputing Center at the University of Science and Technology of China, China.

REFERENCES

(1) Kochuveedu, S. T.; Jang, Y. H.; Kim, D. H. A Study on the Mechanism for the Interaction of Light with Noble Metal-Metal Oxide Semiconductor Nanostructures for Various Photophysical Applications. *Chem. Soc. Rev.* **2013**, *42*, 8467−8493.

(2) Li, X. C.; Zheng, W. J.; He, G. H.; Zhao, R.; Liu, D. Morphology Control of TiO_2 Nanoparticle in Microemulsion and Its Photocatalytic Property. *ACS Sustainable Chem. Eng.* **2014**, *2*, 288−295.

(3) Lang, X.; Ma, W.; Chen, C.; Ji, H.; Zhao, J. Selective Aerobic Oxidation Mediated by TiO_2 Photocatalysis. *Acc. Chem. Res.* **2014**, *47*, 355−363.

(4) Hong, Y. L.; Jing, X. L.; Huang, J. L.; Sun, D. H.; Odoom-Wubah, T.; Yang, F.; Du, M. M.; Li, Q. B. Biosynthesized Bimetallic Au-Pd Nanoparticles Supported on TiO_2 for Solvent-Free Oxidation of Benzyl Alcohol. *ACS Sustainable Chem. Eng.* **2014**, *2*, 1752−1759.

(5) Chen, C. C.; Ma, W. H.; Zhao, J. C. Semiconductor-Mediated Photodegradation of Pollutants under Visible-Light Irradiation. *Chem. Soc. Rev.* **2010**, *39*, 4206−4219.

(6) Fujishima, A.; Honda, K. Electrochemical Photolysis of Water at a Semiconductor Electrode. *Nature* **1972**, *238*, 37−38.

(7) Pu, Y. C.; Wang, G. M.; Chang, K. D.; Ling, Y. C.; Lin, Y. K.; Fitzmorris, B. C.; Liu, C. M.; Lu, X. H.; Tong, Y. X.; Zhang, J. Z.; Hsu, Y. J.; Li, Y. Au Nanostructure-Decorated TiO_2 Nanowires Exhibiting Photoactivity across Entire Uv-Visible Region for Photoelectrochemical Water Splitting. *Nano Lett.* **2013**, *13*, 3817−3823.

(8) Jiang, X.; Fu, X.; Zhang, L.; Meng, S.; Chen, S. Photocatalytic Reforming of Glycerol for H_2 Evolution on Pt/TiO_2: Fundamental Understanding the Effect of Co-Catalyst Pt and the Pt Deposition Route. *J. Mater. Chem. A* **2015**, *3*, 2271−2282.

(9) Subramanian, V.; Wolf, E. E.; Kamat, P. V. Catalysis with TiO_2/Gold Nanocomposites. Effect of Metal Particle Size on the Fermi Level Equilibration. *J. Am. Chem. Soc.* **2004**, *126*, 4943−4950.

(10) Jakob, M.; Levanon, H.; Kamat, P. V. Charge Distribution between Uv-Irradiated TiO_2 and Gold Nanoparticles: Determination of Shift in the Fermi Level. *Nano Lett.* **2003**, *3*, 353−358.

(11) Wu, Y.; Liu, H.; Zhang, J.; Chen, F. Enhanced Photocatalytic Activity of Nitrogen-Doped Titania by Deposited with Gold. *J. Phys. Chem. C* **2009**, *113*, 14689−14695.

(12) Tanaka, A.; Sakaguchi, S.; Hashimoto, K.; Kominami, H. Preparation of Au/TiO_2 with Metal Cocatalysts Exhibiting Strong Surface Plasmon Resonance Effective for Photoinduced Hydrogen Formation under Irradiation of Visible Light. *ACS Catal.* **2013**, *3*, 79−85.

(13) Linic, S.; Christopher, P.; Ingram, D. B. Plasmonic-Metal Nanostructures for Efficient Conversion of Solar to Chemical Energy. *Nat. Mater.* **2011**, *10*, 911−921.

(14) Tian, Y.; Tatsuma, T. Mechanisms and Applications of Plasmon-Induced Charge Separation at TiO_2 Films Loaded with Gold Nanoparticles. *J. Am. Chem. Soc.* **2005**, *127*, 7632−7637.

(15) Furube, A.; Du, L.; Hara, K.; Katoh, R.; Tachiya, M. Ultrafast Plasmon-Induced Electron Transfer from Gold Nanodots into TiO_2 Nanoparticles. *J. Am. Chem. Soc.* **2007**, *129*, 14852−14853.

(16) Naya, S.; Teranishi, M.; Isobe, T.; Tada, H. Light Wavelength-Switchable Photocatalytic Reaction by Gold Nanoparticle-Loaded Titanium(IV) Dioxide. *Chem. Commun.* **2010**, *46*, 815−817.

(17) Zhou, X. M.; Liu, G.; Yu, J. G.; Fan, W. H. Surface Plasmon Resonance-Mediated Photocatalysis by Noble Metal-Based Composites under Visible Light. *J. Mater. Chem.* **2012**, *22*, 21337−21354.

(18) Yan, J.; Wu, G.; Dai, W.; Guan, N.; Li, L. Synthetic Design of Gold Nanoparticles on Anatase TiO_2 {001} for Enhanced Visible Light Harvesting. *ACS Sustainable Chem. Eng.* **2014**, *2*, 1940−1946.

(19) Kim, J.; Lee, J.; Choi, W. Synergic Effect of Simultaneous Fluorination and Platinization of TiO_2 Surface on Anoxic Photocatalytic Degradation of Organic Compounds. *Chem. Commun.* **2008**, 756−758.

(20) Lee, J. S.; Choi, W. Y. Photocatalytic Reactivity of Surface Platinized TiO_2: Substrate Specificity and the Effect of Pt Oxidation State. *J. Phys. Chem. B* **2005**, *109*, 7399−7406.

(21) Wang, C. Y.; Pagel, R.; Bahnemann, D. W.; Dohrmann, J. K. Quantum Yield of Formaldehyde Formation in the Presence of Colloidal TiO_2-Based Photocatalysts: Effect of Intermittent Illumination, Platinization, and Deoxygenation. *J. Phys. Chem. B* **2004**, *108*, 14082−14092.

(22) Tada, H.; Kiyonaga, T.; Naya, S. Rational Design and Applications of Highly Efficient Reaction Systems Photocatalyzed by Noble Metal Nanoparticle-Loaded Titanium(IV) Dioxide. *Chem. Soc. Rev.* **2009**, *38*, 1849−1858.

(23) Xue, J. J.; Ma, S. S.; Zhou, Y. M.; Zhang, Z. W.; He, M. Facile Photochemical Synthesis of $Au/Pt/G\text{-}C_3N_4$ with Plasmon-Enhanced Photocatalytic Activity for Antibiotic Degradation. *ACS Appl. Mater. Interfaces* **2015**, *7*, 9630−9637.

(24) Naldoni, A.; D'Arienzo, M.; Altomare, M.; Marelli, M.; Scotti, R.; Morazzoni, F.; Selli, E.; Dal Santo, V. Pt and Au/TiO_2 Photocatalysts for Methanol Reforming: Role of Metal Nanoparticles in Tuning Charge Trapping Properties and Photoefficiency. *Appl. Catal., B* **2013**, *130−131*, 239−248.

(25) Yang, H. G.; Sun, C. H.; Qiao, S. Z.; Zou, J.; Liu, G.; Smith, S. C.; Cheng, H. M.; Lu, G. Q. Anatase TiO_2 Single Crystals with a Large Percentage of Reactive Facets. *Nature* **2008**, *453*, 638−641.

(26) Yuan, S. J.; Chen, J. J.; Lin, Z. Q.; Li, W. W.; Sheng, G. P.; Yu, H. Q. Nitrate Formation from Atmospheric Nitrogen and Oxygen Photocatalysed by Nano-Sized Titanium Dioxide. *Nat. Commun.* **2013**, *4*, 2249.

DOI: 10.1021/acsami.5b06161
ACS Appl. Mater. Interfaces 2015, 7, 20349−20359

(27) Anandan, S.; Rao, T. N.; Sathish, M.; Rangappa, D.; Honma, I.; Miyauchi, M. Superhydrophilic Graphene-Loaded TiO_2 Thin Film for Self-Cleaning Applications. *ACS Appl. Mater. Interfaces* **2013**, *5*, 207−212.
(28) Hanson, K.; Losego, M. D.; Kalanyan, B.; Ashford, D. L.; Parsons, G. N.; Meyer, T. J. Stabilization of $[Ru(Bpy)_2(4,4'-(PO_3H_2)Bpy)]^{2+}$ on Mesoporous TiO_2 with Atomic Layer Deposition of Al_2O_3. *Chem. Mater.* **2013**, *25*, 3−5.
(29) Li, X.; Yu, J.; Low, J.; Fang, Y.; Xiao, J.; Chen, X. Engineering Heterogeneous Semiconductors for Solar Water Splitting. *J. Mater. Chem. A* **2015**, *3*, 2485−2534.
(30) Lazzeri, M.; Vittadini, A.; Selloni, A. Structure and Energetics of Stoichiometric TiO_2 Anatase Surfaces. *Phys. Rev. B: Condens. Matter Mater. Phys.* **2001**, *63*, 155409.
(31) Liu, G.; Yang, H. G.; Pan, J.; Yang, Y. Q.; Lu, G. Q.; Cheng, H. M. Titanium Dioxide Crystals with Tailored Facets. *Chem. Rev.* **2014**, *114*, 9559−9612.
(32) Han, X. G.; Zheng, B. J.; Ouyang, J. J.; Wang, X.; Kuang, Q.; Jiang, Y. Q.; Xie, Z. X.; Zheng, L. S. Control of Anatase TiO_2 Nanocrystals with a Series of High-Energy Crystal Facets Via a Fuorine-Free Strategy. *Chem. - Asian J.* **2012**, *7*, 2538−2542.
(33) Chong, R. F.; Li, J.; Zhou, X.; Ma, Y.; Yang, J. X.; Huang, L.; Han, H. X.; Zhang, F. X.; Li, C. Selective Photocatalytic Conversion of Glycerol to Hydroxyacetaldehyde in Aqueous Solution on Facet Tuned TiO_2-Based Catalysts. *Chem. Commun.* **2014**, *50*, 165−167.
(34) Chen, W.; Kuang, Q.; Wang, Q. X.; Xie, Z. X. Engineering a High Energy Surface of Anatase TiO_2 Crystals Towards Enhanced Performance for Energy Conversion and Environmental Applications. *RSC Adv.* **2015**, *5*, 20396−20409.
(35) De Angelis, F.; Vitillaro, G.; Kavan, L.; Nazeeruddin, M. K.; Gratzel, M. Modeling Ruthenium-Dye-Sensitized TiO_2 Surfaces Exposing the (001) or (101) Faces: A First-Principles Investigation. *J. Phys. Chem. C* **2012**, *116*, 18124−18131.
(36) Luan, Y. B.; Jing, L. Q.; Xie, Y.; Sun, X. J.; Feng, Y. J.; Fu, H. G. Exceptional Photocatalytic Activity of 001-Facet-Exposed TiO_2 Mainly Depending on Enhanced Adsorbed Oxygen by Residual Hydrogen Fluoride. *ACS Catal.* **2013**, *3*, 1378−1385.
(37) Li, C.; Koenigsmann, C.; Ding, W.; Rudshteyn, B.; Yang, K. R.; Regan, K. P.; Konezny, S. J.; Batista, V. S.; Brudvig, G. W.; Schmuttenmaer, C. A.; Kim, J.-H. Facet-Dependent Photoelectrochemical Performance of TiO_2 Nanostructures: An Experimental and Computational Study. *J. Am. Chem. Soc.* **2015**, *137*, 1520−1529.
(38) Roy, N.; Sohn, Y.; Pradhan, D. Synergy of Low-Energy (101) and High-Energy (001) TiO_2 Crystal Facets for Enhanced Photocatalysis. *ACS Nano* **2013**, *7*, 2532−2540.
(39) Jo, W. K.; Won, Y.; Hwang, I.; Tayade, R. J. Enhanced Photocatalytic Degradation of Aqueous Nitrobenzene Using Graphitic Carbon-TiO_2 Composites. *Ind. Eng. Chem. Res.* **2014**, *53*, 3455−3461.
(40) Tayade, R. J.; Kulkarni, R. G.; Jasra, R. V. Photocatalytic Degradation of Aqueous Nitrobenzene by Nanocrystalline TiO_2. *Ind. Eng. Chem. Res.* **2006**, *45*, 922−927.
(41) Kamegawa, T.; Seto, H.; Matsuura, S.; Yamashita, H. Preparation of Hydroxynaphthalene-Modified TiO_2 Via Formation of Surface Complexes and Their Applications in the Photocatalytic Reduction of Nitrobenzene under Visible-Light Irradiation. *ACS Appl. Mater. Interfaces* **2012**, *4*, 6635−6639.
(42) Tada, H.; Ishida, T.; Takao, A.; Ito, S. Drastic Enhancement of TiO_2-Photocatalyzed Reduction of Nitrobenzene by Loading Ag Clusters. *Langmuir* **2004**, *20*, 7898−7900.
(43) Cropek, D.; Kemme, P. A.; Makarova, O. V.; Chen, L. X.; Rajh, T. Selective Photocatalytic Decomposition of Nitrobenzene Using Surface Modified TiO_2 Nanoparticles. *J. Phys. Chem. C* **2008**, *112*, 8311−8318.
(44) Makarova, O. V.; Rajh, T.; Thurnauer, M. C.; Martin, A.; Kemme, P. A.; Cropek, D. Surface Modification of TiO_2 Nanoparticles for Photochemical Reduction of Nitrobenzene. *Environ. Sci. Technol.* **2000**, *34*, 4797−4803.
(45) Liu, C.; Han, X. G.; Xie, S. F.; Kuang, Q.; Wang, X.; Jin, M. S.; Xie, Z. X.; Zheng, L. S. Enhancing the Photocatalytic Activity of Anatase TiO_2 by Improving the Specific Facet-Induced Spontaneous Separation of Photogenerated Electrons and Holes. *Chem. - Asian J.* **2013**, *8*, 282−289.
(46) Gao, S.; Wang, W.; Ni, Y.; Lu, C.; Xu, Z. Facet-Dependent Photocatalytic Mechanisms of Anatase TiO_2: A New Sight on the Self-Adjusted Surface Heterojunction. *J. Alloys Compd.* **2015**, *647*, 981−988.
(47) Nie, L. H.; Yu, J. G.; Li, X. Y.; Cheng, B.; Liu, G.; Jaroniec, M. Enhanced Performance of Naoh-Modified Pt/TiO_2 toward Room Temperature Selective Oxidation of Formaldehyde. *Environ. Sci. Technol.* **2013**, *47*, 2777−2783.
(48) Zhang, P.; Tachikawa, T.; Bian, Z. F.; Majima, T. Selective Photoredox Activity on Specific Facet-Dominated TiO_2 Mesocrystal Superstructures Incubated with Directed Nanocrystals. *Appl. Catal., B* **2015**, *176−177*, 678−686.
(49) Chen, J.-J.; Wang, W.-K.; Li, W.-W.; Pei, D.-N.; Yu, H.-Q. Roles of Crystal Surface in Pt-Loaded Titania for Photocatalytic Conversion of Organic Pollutants: A First-Principle Theoretical Calculation. *ACS Appl. Mater. Interfaces* **2015**, *7*, 12671−12678.
(50) Surolia, P. K.; Tayade, R. J.; Jasra, R. V. Photocatalytic Degradation of Nitrobenzene in an Aqueous System by Transition-Metal-Exchanged ETS-10 Zeolites. *Ind. Eng. Chem. Res.* **2010**, *49*, 3961−3966.
(51) Wahab, H. S.; Koutselos, A. D. Computational Modeling of the Adsorption and (*)Oh Initiated Photochemical and Photocatalytic Primary Oxidation of Nitrobenzene. *J. Mol. Model.* **2009**, *15*, 1237−1244.
(52) Khan, S. U. M.; Al-Shahry, M.; Ingler, W. B., Jr. Efficient Photochemical Water Splitting by a Chemically Modified N-TiO_2. *Science* **2002**, *297*, 2243−2245.
(53) Barnard, A. S.; Curtiss, L. A. Prediction of TiO_2 Nanoparticle Phase and Shape Transitions Controlled by Surface Chemistry. *Nano Lett.* **2005**, *5*, 1261−1266.
(54) Bourikas, K.; Kordulis, C.; Lycourghiotis, A. Titanium Dioxide (Anatase and Rutile): Surface Chemistry, Liquid Solid Interface Chemistry, and Scientific Synthesis of Supported Catalysts. *Chem. Rev.* **2014**, *114*, 9754−9823.
(55) Yu, Y.; Cao, C. Y.; Li, W.; Li, P.; Qu, J.; Song, W. G. Low-Cost Synthesis of Robust Anatase Polyhedral Structures with a Preponderance of Exposed (001) Facets for Enhanced Photoactivities. *Nano Res.* **2012**, *5*, 434−442.
(56) Zhang, A. Y.; Long, L. L.; Li, W. W.; Wang, W. K.; Yu, H. Q. Hexagonal Microrods of Anatase Tetragonal TiO_2: Self-Directed Growth and Superior Photocatalytic Performance. *Chem. Commun.* **2013**, *49*, 6075−6077.
(57) Yu, J. G.; Low, J. X.; Xiao, W.; Zhou, P.; Jaroniec, M. Enhanced Photocatalytic CO_2-Reduction Activity of Anatase TiO_2 by Coexposed {001} and {101} Facets. *J. Am. Chem. Soc.* **2014**, *136*, 8839−8842.
(58) Liu, G.; Tao, C.; Zhang, M.; Gu, X.; Meng, F.; Zhang, X.; Chen, Y.; Ruan, S. Effects of Surface Self-Assembled NH_4^+ on the Performance of TiO_2-Based Ultraviolet Photodetectors. *J. Alloys Compd.* **2014**, *601*, 104−107.
(59) Brunauer, S.; Deming, L. S.; Deming, W. E.; Teller, E. On a Theory of the Van Der Waals Adsorption of Gases. *J. Am. Chem. Soc.* **1940**, *62*, 1723−1732.
(60) Sing, K. S. W.; Everett, D. H.; Haul, R. A. W.; Moscou, L.; Pierotti, R. A.; Rouquerol, J.; Siemieniewska, T. Reporting Physisorption Data for Gas Solid Systems with Special Reference to the Determination of Surface-Area and Porosity (Recommendations 1984). *Pure Appl. Chem.* **1985**, *57*, 603−619.
(61) Li, Y. H.; Xing, J.; Chen, Z. J.; Li, Z.; Tian, F.; Zheng, L. R.; Wang, H. F.; Hu, P.; Zhao, H. J.; Yang, H. G. Unidirectional Suppression of Hydrogen Oxidation on Oxidized Platinum Clusters. *Nat. Commun.* **2013**, *4*, 2500.
(62) Sheng, Y. G.; Liang, L. P.; Xu, Y.; Wu, D.; Sun, Y. H. Low-Temperature Deposition of the High-Performance Anatase-Titania Optical Films Via a Modified Sol-Gel Route. *Opt. Mater.* **2008**, *30*, 1310−1315.

DOI: 10.1021/acsami.5b06161
ACS Appl. Mater. Interfaces 2015, 7, 20349−20359

(63) Wang, S.; Zhao, L.; Bai, L. N.; Yan, J. M.; Jiang, Q.; Lian, J. S. Enhancing Photocatalytic Activity of Disorder-Engineered C/TiO_2 and TiO_2 Nanoparticles. *J. Mater. Chem. A* **2014**, *2*, 7439−7445.
(64) Fan, C. Y.; Chen, C.; Wang, J.; Fu, X. X.; Ren, Z. M.; Qian, G. D.; Wang, Z. Y. Black Hydroxylated Titanium Dioxide Prepared Via Ultrasonication with Enhanced Photocatalytic Activity. *Sci. Rep.* **2015**, *5*, 11712.
(65) Schneider, J.; Matsuoka, M.; Takeuchi, M.; Zhang, J. L.; Horiuchi, Y.; Anpo, M.; Bahnemann, D. W. Understanding TiO_2 Photocatalysis: Mechanisms and Materials. *Chem. Rev.* **2014**, *114*, 9919−9986.
(66) Zhang, Z.; Yates, J. T. Band Bending in Semiconductors: Chemical and Physical Consequences at Surfaces and Interfaces. *Chem. Rev.* **2012**, *112*, 5520−5551.
(67) Luber, E. J.; Buriak, J. M. Reporting Performance in Organic Photovoltaic Devices. *ACS Nano* **2013**, *7*, 4708−4714.
(68) Zhang, S. J.; Jiang, H.; Li, M. J.; Yu, H. Q.; Yin, H.; Li, Q. R. Kinetics and Mechanisms of Radiolytic Degradation of Nitrobenzene in Aqueous Solutions. *Environ. Sci. Technol.* **2007**, *41*, 1977−1982.
(69) Tachikawa, T.; Yamashita, S.; Majima, T. Evidence for Crystal-Face-Dependent TiO_2 Photocatalysis from Single-Molecule Imaging and Kinetic Analysis. *J. Am. Chem. Soc.* **2011**, *133*, 7197−7204.

DOI: 10.1021/acsami.5b06161
ACS Appl. Mater. Interfaces 2015, 7, 20349−20359